

Observations of fresh, anticyclonic eddies in the Hudson Strait outflow

David A. Sutherland ^{a*}
Fiammetta Straneo ^b
Steven J. Lentz ^b
Pierre Saint-Laurent ^c

Draft, November 2009, Not Submitted yet

*corresponding author

^a School of Oceanography
University of Washington
Box 355351
Seattle, WA 98195-5351
dsuth@uw.edu

^b Department of Physical Oceanography
Woods Hole Oceanographic Institution
MS #21
Woods Hole, MA 02543

^c Institut des Sciences de la Mer
Université of Québec à Rimouski
310, allée des Ursulines
Rimouski, QC, G5L 3A1, Canada

1 **Abstract**

2 The waters that flow out through Hudson Strait, a coastal system that connects Hudson
3 Bay with the Labrador Sea, constitute the third largest freshwater contribution to the northern
4 North Atlantic, behind only Fram Strait and Davis Strait. Recent studies have documented the
5 mean structure and transport of the outflow, as well as highlighting significant variability on
6 synoptic (days to a week) scales. This study examines the variability of the outflow on these
7 synoptic scales through the use of an unprecedented set of observations collected by a mooring
8 array from 2005-2006 in the strait. In particular, we focus on the mechanisms that cause the
9 freshwater export to be concentrated in a series of discrete pulses during the fall/winter season.
10 We show that these freshwater pulses, which occur once every 4.4 days on average, are
11 anticyclonic, surface-trapped eddies propagating through the strait and carried by the mean
12 outflow. Their occurrence is related to the passage of storms across Hudson Bay, although local
13 instability processes could also play a role in their formation. The eddies are responsible for
14 approximately 40% of the mean volume transport and 50% of the mean freshwater transport out
15 of the strait. We discuss the implications of this new freshwater release mechanism on the
16 delivery of nutrient-rich and highly stratified waters to the Labrador shelf, a highly productive
17 region south of Hudson Strait.

18

19 **Keywords:** Hudson Strait, Hudson Bay, Labrador Current, freshwater

20

21 **Index terms:**

22

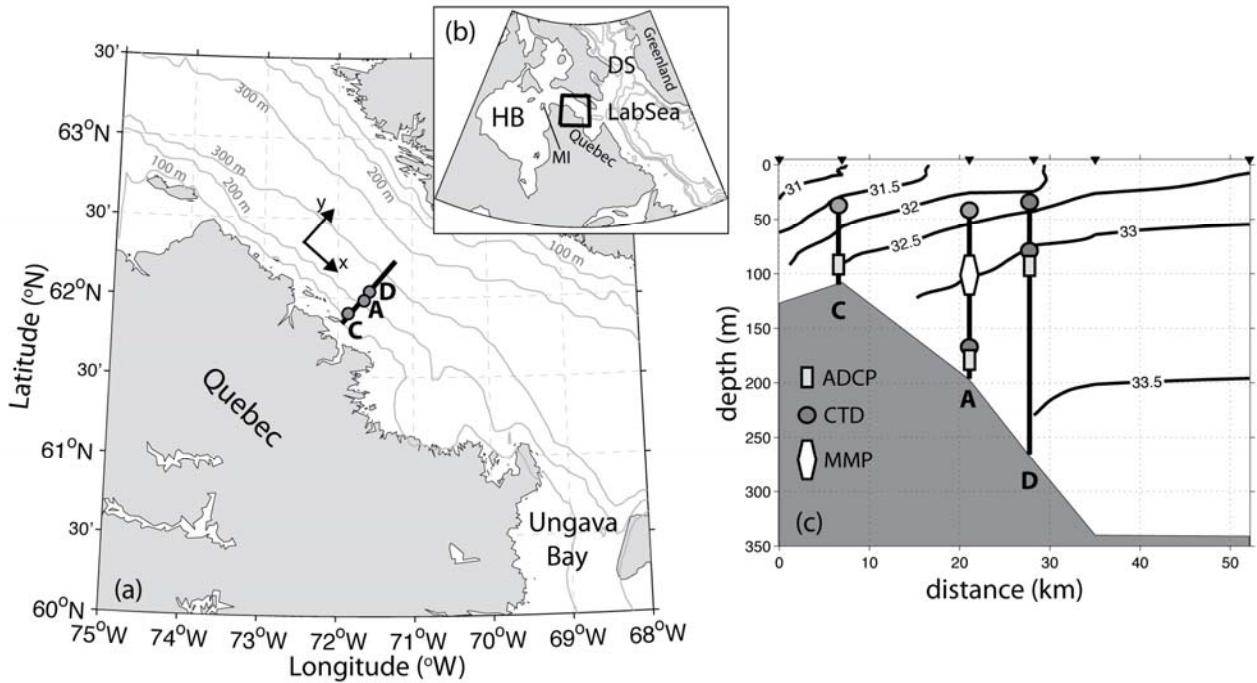
23 **1. Introduction**

24 Observational efforts in the Arctic and subarctic seas have intensified in the last decade
25 (e.g., Dickson *et al.*, 2008), with the goal of obtaining a baseline knowledge of the freshwater
26 pathways in the high-latitude oceans, which are expected to change significantly in any future
27 climate change scenario. These efforts have resulted in more accurate and up-to-date estimates of
28 the major freshwater budget terms (Serreze *et al.*, 2006; Dickson *et al.*, 2007), and, in some
29 regions, led to new insights on the distribution and variability in freshwater storage.

30 One example is Hudson Strait, a 100 km wide, 400 km long channel with mean depths of
31 ~300 m (Fig. 1) that connects Hudson Bay with the Labrador Sea. The Hudson Strait outflow is a
32 baroclinic, buoyancy-driven current on the southern side of the channel (Fig. 1c), with a width of
33 ~30 km and a depth of ~120 m (Straneo and Saucier, 2008a; Ingram and Prisenberg, 1998;
34 Drinkwater, 1988). This mean structure is primarily the result of the large river input into the
35 Hudson Bay system, ~900 km³ yr⁻¹ (Déry *et al.*, 2005), that sets up the buoyant current in
36 roughly semigeostrophic balance (Straneo and Saucier, 2008a; Lentz and Largier, 2006), while
37 the mean downwelling favorable winds in the strait aid in keeping the outflow coherent against
38 the Quebec coast. The outflow represents the third largest net source of freshwater to the North
39 Atlantic Ocean, behind only the flow through Fram and Davis Straits from the Arctic Ocean. The
40 freshwater transport exhibits a strong seasonal cycle, with increased discharge exiting through
41 the Strait from October to April presumably due to the timing of river input into Hudson Bay, as
42 well as modification by the melt/freeze cycle of sea ice in the area (Ingram and Prisenberg, 1998;
43 Straneo and Saucier, 2008b; Saucier *et al.*, 2004).

44 On the northern side, a barotropic inflow brings Baffin Bay and Davis Strait water into
45 the strait, where it either re-circulates by mixing with the Hudson Strait outflow or passes into

46 Hudson Bay itself, eventually exiting a few years later (Straneo and Saucier, 2008a; Saucier *et*
 47 *al.*, 2004). The reprocessing and mixing of Davis Strait water with Hudson Strait water results in
 48 a mean freshwater transport of 78-88 mSv (reference salinity 34.8) flowing out of Hudson Strait
 49 onto the Labrador Shelf, making up approximately 50% of the total Labrador current freshwater
 50 transport (Straneo and Saucier, 2008a,b).



51 **Figure 1.** (a) Mooring locations (C, A, D) for the 2005-2006 deployment in the Hudson Strait outflow
 52 region. The solid line indicates the location of the CTD section displayed in c. (b) Regional map showing
 53 the location of Hudson Strait with respect to the larger Hudson Bay system (HB), the Labrador Sea, and
 54 Davis Strait (DS). The star marks the location of the wind data used for Hudson Bay, south of Mansel
 55 Island (MI). (c) Salinity section from a CTD transect (stations marked by black triangles) occupied in
 56 September 2005 along the line shown in a. The mooring locations are superimposed with schematic
 57 representations of instrument depths and types.
 58
 59

60 In addition to its critical role in the high-latitude freshwater budget, the Hudson Strait
 61 outflow is also the primary conduit of high nutrient waters to the Labrador shelf. These nutrients
 62 are thought to greatly contribute to the high productivity and fish abundance over the Labrador
 63 shelf (e.g., Sutcliffe *et al.*, 1983; Drinkwater and Harding, 2001).

64 Within the seasonal envelope of increased freshwater transport through the strait, though,
65 observations display large variations in velocity and salinity on synoptic timescales (several days
66 to a week), but with an entirely unknown origin (Straneo and Saucier, 2008*a*; Drinkwater, 1988).
67 The main goal of the present work is to investigate these higher frequency, synoptic-scale
68 variations in the Hudson Strait outflow, in contrast to previous work that focused on its mean and
69 seasonal structure (Drinkwater, 1988; Straneo and Saucier, 2008*a,b*). Using a set of moored
70 observations across the strait over one year, we show that these high frequency events carry a
71 significant fraction of the freshwater and volume transport of the Hudson Strait outflow. This
72 puts into question the conventional view of the outflow as a continuous release of freshwater
73 from Hudson Bay. Indeed, we propose that the mechanism for freshwater release from Hudson
74 Bay is via a discrete series of pulses that carry low-salinity waters with a high river-water content
75 through Hudson Strait. The coherence of these pulses, which keeps the waters inside them
76 weakly mixed and with more of their original Hudson Bay characteristics intact, has implications
77 for the downstream stratification and productivity of the Labrador Current.

78 We do not ignore variability on shorter time scales, such as induced by tides, since tidal
79 ranges in Hudson Strait can reach 8 m and play an important role in mixing (e.g., Egbert and
80 Ray, 2001; Arbic *et al.*, 2007), but we show that they do not control the variability observed on
81 synoptic scales. We accomplish this by utilizing a one-year long observational data set, outlined
82 in section 2 below, to support the proposed hypothesis above that the freshwater transport
83 mechanism is dominated by a series of low-salinity pulses that occur on synoptic timescales
84 (section 3). The processes responsible for the formation and propagation of these low-salinity
85 signals, as well as evidence of their origin, are discussed in section 4.

86

87 2. Data

88 A set of three moorings was deployed in the outflow region of Hudson Strait from
89 summer 2004 to summer 2007 and represents the first successful three-year mooring record from
90 the strait (Fig. 1). Here we focus on the second deployment year, 2005-2006; details of the
91 processing, calibration, and mooring design for the first year, 2004-2005, can be found in
92 Straneo and Saucier (2008a) and for the third year in Straneo *et al.* (2010). Here we limit our
93 analysis to the second year of data since it contains the only full depth and time record of
94 hydrographic observations at the central mooring, velocity measurements across the mooring
95 array, and additional instruments measuring fluorescence and sea ice draft (see below). The
96 spacing of the mooring array across the strait was changed from 2004-2005 to fully capture the
97 outflow, which has a mean maximum velocity centered near mooring A, oriented at an angle
98 125° along the bathymetry towards the southeast (Fig. 1a). This central mooring was also
99 equipped with an Upward Looking Sonar (ULS) at 46 m depth that measured pressure, tilt, and
100 sea ice draft, and was situated shallower than the previous year to account for the removal of the
101 Arctic Winch system (Straneo and Saucier, 2008a).

102

103 2.1 Velocity data and processing

104 Each mooring was equipped with an upward looking Acoustic Doppler Current Profiler
105 (ADCP) situated near-bottom at mooring A (water depth ~ 171 m) and C (90 m), and at a depth
106 of 77 m at mooring D (260 m), shown in Fig. 1c. The central mooring had a RDI 75 kHz long-
107 range ADCP (10 m bins, 15 min. sampling), while the outer moorings were equipped with 300
108 kHz RDI sensors (4 m bins, 15 min. sampling). Velocities in the upper 20 m were blanked out at
109 each location to reduce errors from surface effects, as well as to reduce impact of the large tidal

110 range present (~8 m). Tidal velocities were estimated using the T-Tide package in MATLAB
111 (Pawlowicz *et al.*, 2002), and then subtracted out. The detided velocities were then filtered with a
112 34-hr low-pass filter to remove any residual tidal signal. Adjustments were also made for the
113 magnetic declinations of 29°W, 29.2°W, and 28.4°W for each ADCP at moorings A, D, and C,
114 respectively.

115 Finally, the corrected, detided velocities were rotated into along- and across-strait
116 directions using an angle of 125° (Fig. 1a). This angle was chosen as a mean bathymetric angle
117 and corresponds well to the angle of maximum current variance observed, although each
118 mooring location varied by several degrees around 125°. Throughout the rest of the paper, we
119 refer to these processed, detided, and rotated velocities, U_{along} and U_{across} , simply as along- and
120 across-strait velocities.

121 Data return from the ADCPs were good during 2005-2006, except at mooring A, where a
122 software malfunction limited the data to a 4 month period, Sept. 10, 2005-Jan. 10, 2006. Along-
123 strait velocities after the malfunction were estimated in two ways. The first method uses the ULS
124 tilt sensor to derive an empirical relation between velocity and tilt at each depth when there was
125 data, and then uses that relation to calculate velocities after Jan. 10, 2006, exactly as *Straneo and*
126 *Saucier* (2008a) did after a similar malfunction in year 1. The second method compares U_{along} at
127 mooring A with those at C and D, deriving linear fits between them at each common depth, and
128 then using those to calculate velocities at A when there was no ADCP data. Both methods gave
129 similar results, though the second method was good only to the deepest depth of C and D, ~77 m.
130 Therefore, for the time-period after Jan. 10, 2006, we use the tilt-derived velocities for U_{along} at
131 mooring A. We emphasize though that these velocities are not critical to the analysis presented

132 here focusing on synoptic-scale variability mechanisms, and the conclusions do not depend upon
133 the actual values calculated.

134

135 *2.2 Hydrographic data and processing*

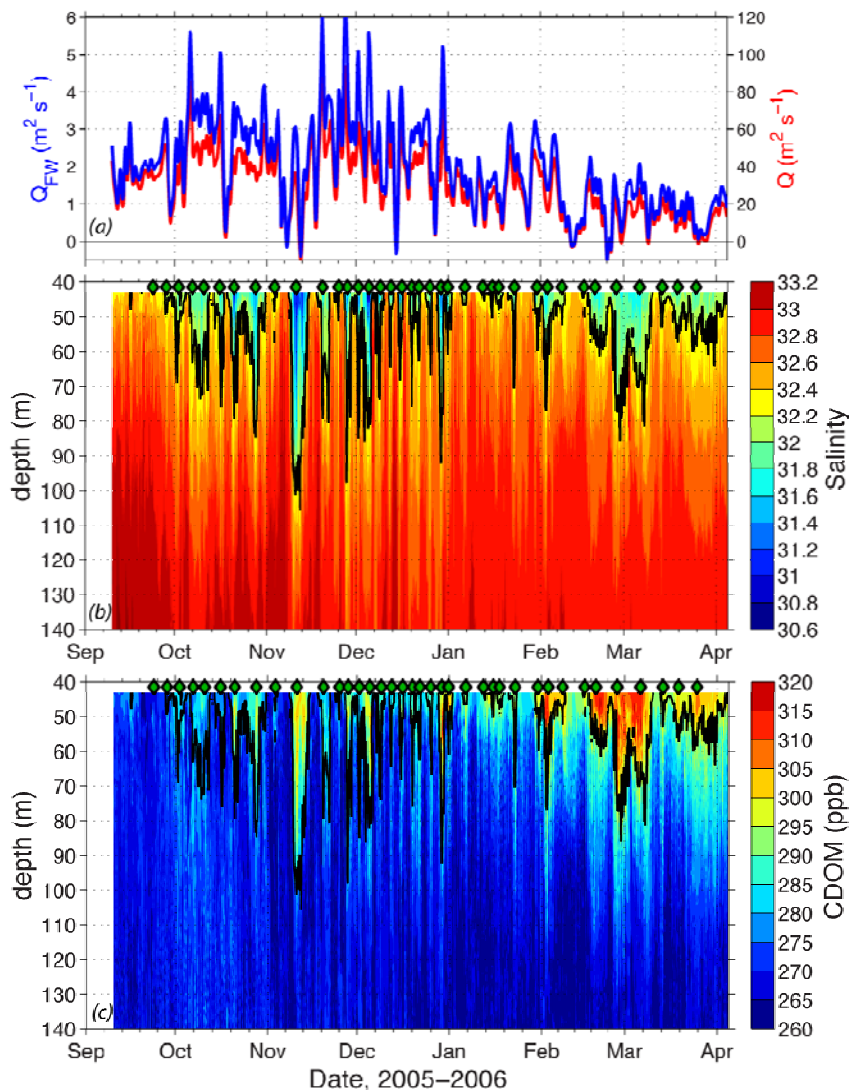
136 Each mooring was equipped with a set of instruments to measure hydrographic properties
137 (Fig. 1c). Mooring A was the most heavily instrumented, with an upper (46 m) and lower (171
138 m) Seabird SBE37 MicroCat conductivity, temperature, depth recorder (CTD) measuring salinity
139 (S), temperature (T), and pressure at fixed locations, as well as a McLane Moored Profiler
140 (MMP) that ranged from ~46-170 m along the mooring. The MMP collected profiles of S , T ,
141 pressure, and chromophoric dissolved organic matter (CDOM) fluorescence, at an average
142 interval of every 4 hours, while the CTDs recorded every 30 minutes. The outer mooring, D, also
143 had an upper (27 m) and lower (77 m) CTD recording every 30 minutes. Unfortunately, the CTD
144 placed on mooring C (41 m) failed, and no hydrographic data were recovered for this location
145 during this year.

146 All of the CTDs were calibrated before deployment and post-recovery calibration was
147 handled using hydrographic casts taken during the recovery, or by comparison to nearby
148 instruments. The MMP data were interpolated to a regular grid in time (5 points per day) and in
149 the vertical (2 m spacing). CTD data were subsampled in time to every hour to facilitate simpler
150 data analysis. The MMP and CTD measurements of S and T at mooring A were combined to
151 extend the vertical range of the observations to ~40-180 m (see Fig. 2).

152 In addition to the mooring data, hydrographic stations across the strait were occupied
153 during each mooring deployment/recovery cruise, and provide snapshots of the outflow region

154 (e.g., in September 2005 shown in Fig. 1c). For 2005, the observations were obtained using a 24-
 155 bottle rosette with a Seabird CTD on the Canadian Coast Guard vessel *CCGS Pierre Radisson*.

156 Meteorological variables over the strait and in eastern Hudson Bay were obtained from
 157 the six-hourly, $2.5^\circ \times 2.5^\circ$ resolution NCEP reanalysis fields (<http://www.cdc.noaa.gov/>). In
 158 particular, we used the 10-m zonal and meridional winds (U_{wind} , V_{wind}) interpolated to a position
 159 inside the strait near mooring A (61.98°N , 71.64°W) and over the entire Hudson Bay.



160
 161 **Figure 2.** (a) Observed freshwater transport (per unit width, relative to $S = 34.8$, in blue) and volume
 162 transport (per unit width, red) of the Hudson Strait outflow, calculated at mooring A. (b) Salinity record
 163 from the moored profiler (MMP) at mooring A with the 32.2 isohaline contoured (black) and individual
 164 low-salinity events indicated (green diamonds). (c) Same as in b but for CDOM, with the 32.2 isohaline
 165 contoured (black).

166 **3. Results**

167 The salinity record from the MMP displayed in Fig. 2, combined with the snapshot of the
168 outflow's cross-strait structure (Fig. 1c), illustrates several essential features of the Hudson Strait
169 outflow. On seasonal timescales, the freshest waters ($S < 32.2$) leave Hudson Strait from early
170 October to early January, with additional low-salinity water observed from February to April.
171 However, this secondary pulse is less pronounced in the freshwater transport calculation since it
172 is associated with relatively weak velocities (Fig. 2).

173 On synoptic timescales within this seasonal envelope, the dominant feature in the salinity
174 record is a series of low-salinity pulses lasting from one to several days (Fig. 2b). These low-
175 salinity pulses reach to depths of 100 m. Note that the CTD section shown in Fig. 1c indicates a
176 depth for the 32.2 isohaline at mooring A of roughly 50 m, which is relatively shallow in the
177 context of the yearly salinity record. The CTD section illustrates the cross-strait salinity gradient,
178 $\partial S/\partial y > 0$, that is persistent throughout the year between moorings A and D, but unknown
179 between A and C for 2005-2006 since the CTD instrument failed at the inner mooring. Data from
180 2004-2005 in the same region show that $\partial S/\partial y$ is positive across the entire outflow and
181 intensified in the surface layer, in accordance with the baroclinic nature of the flow (Straneo and
182 Saucier, 2008a).

183 The record of CDOM throughout the water column at mooring A (Fig. 2c) shows a
184 similar seasonal and high frequency variability to the salinity observations. High CDOM
185 corresponds to high river water content, but can be modified by the seasonal sea ice cycle. The
186 highest values of CDOM are confined in time and in the vertical to the freshest salinities, as the
187 32.2 isohaline captures them qualitatively well (Fig. 2c).

188 The freshwater and volume transports calculated at mooring A (Fig. 2a), referenced to a
189 salinity of 34.8 to compare with previous studies and the majority of Arctic freshwater budget
190 calculations, show considerable variability on similar synoptic time scales as the salinity
191 variability. The range of freshwater transport per unit width goes from a minimum just below
192 zero to a maximum near $6 \text{ m}^2 \text{ s}^{-1}$. These extremes in freshwater transport seem to be related to
193 the occurrence of low-salinity events observed by the MMP at mooring A. Thus, to understand
194 what controls the freshwater transport variability, we need to understand the processes behind the
195 synoptic scale variability.

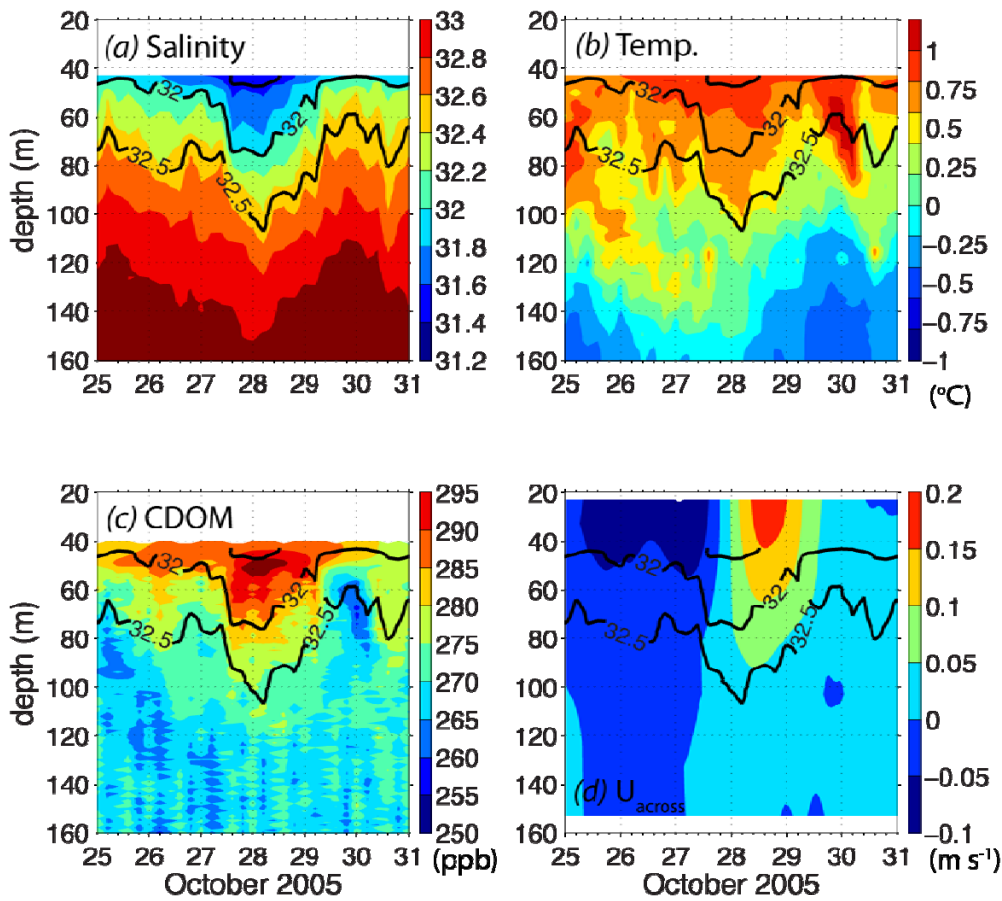
196

197 *3.1 Synoptic-scale variability*

198 Fig. 3 displays a zoom-in of observations taken at mooring A, with S , T , and CDOM from
199 the MMP, and U_{across} from the ADCP, during a 6-day period in late October 2005. The salinity
200 data (Fig. 3a) show the appearance of low-salinity waters with $S < 31.5$ centered near 28-Oct-
201 2005, when the 32.5 isohaline dips to ~ 105 m. After this maximum depth is reached, the
202 isohalines shoal and return to their previous vertical positions. Associated with the presence of
203 the relatively fresh, upper-layer water are relatively higher T (Fig. 3b), higher CDOM
204 concentrations (Fig. 3c), and a reversal in U_{across} from onshore to offshore-directed velocity (Fig.
205 3d). We define the passage of an event occurring when a local minimum in S is reached in the
206 upper water column (~ 40 -60 m) and is coincident with a zero crossing in U_{across} in the same
207 depth range.

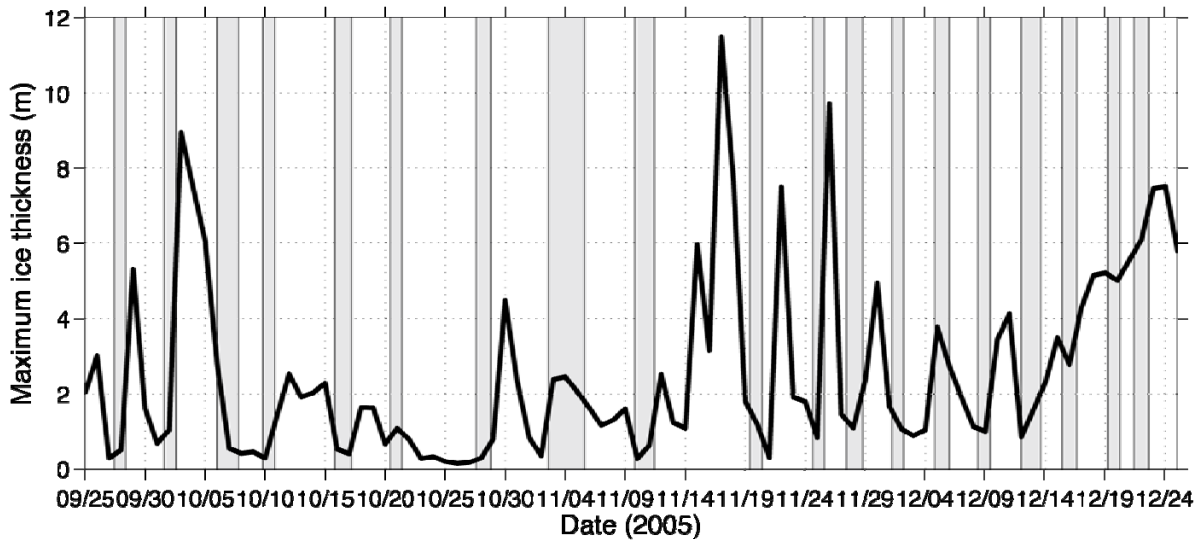
208 Using this definition for a low-salinity event results in 38 identifiable pulses from late
209 September 2005 to early April 2006 (Fig. 2b). Since S varies seasonally, using a local minimum
210 criterion combined with a velocity criterion gave more meaningful results than using a fixed

211 salinity level. Although T and CDOM were not used in defining when an event occurred, they
 212 were coherent with the S and U_{across} signals (Fig. 3) in each identified pulse. On the other hand,
 213 observations of U_{along} and MMP backscatter (not shown) did not show a consistent signal
 214 associated with the occurrence of these low-salinity events. In general there was an increase in
 215 U_{along} associated with each event, but the peak increase did not always exactly match the timing
 216 of the minimum salinity.
 217



218
 219
 220 **Figure 3.** (a) Observed salinity record from the moored profiler (MMP) at mooring A during a typical
 221 low-salinity event that occurred in late October 2005. Select isohalines (black lines: 31.5, 32, 32.5) are
 222 indicated similarly across all panels. (b) Same as in a, but for the observed temperature record from the
 223 MMP. (c) Same as in a, but for the observed CDOM record from the MMP fluorometer. (d) Across-strait
 224 velocity ($U_{across} < 0$ is onshore) for the same time period as in a-c, from the ADCP at mooring A.
 225

226 The occurrence of these low-salinity pulses was also observed in the sea ice data from the
 227 ULS located on the central mooring, shown in Fig. 4. Ice covers Hudson Strait from early winter
 228 (~December) to spring (~April), and throughout the fall months, large pieces of sea ice from
 229 northern Hudson Bay, such as Foxe Basin, can be observed in the strait outflow (Gagnon and
 230 Gough, 2005). The pulses, however, are not associated with these but are, instead, associated
 231 with a minimum in sea-ice draft (using the mean ice draft gives a similar result). A correlation of
 232 the upper water column salinity (as a proxy for the low-salinity events) and the maximum ice
 233 thickness results in a positive correlation coefficient of 0.35, which is significant at the 95%
 234 level.
 235



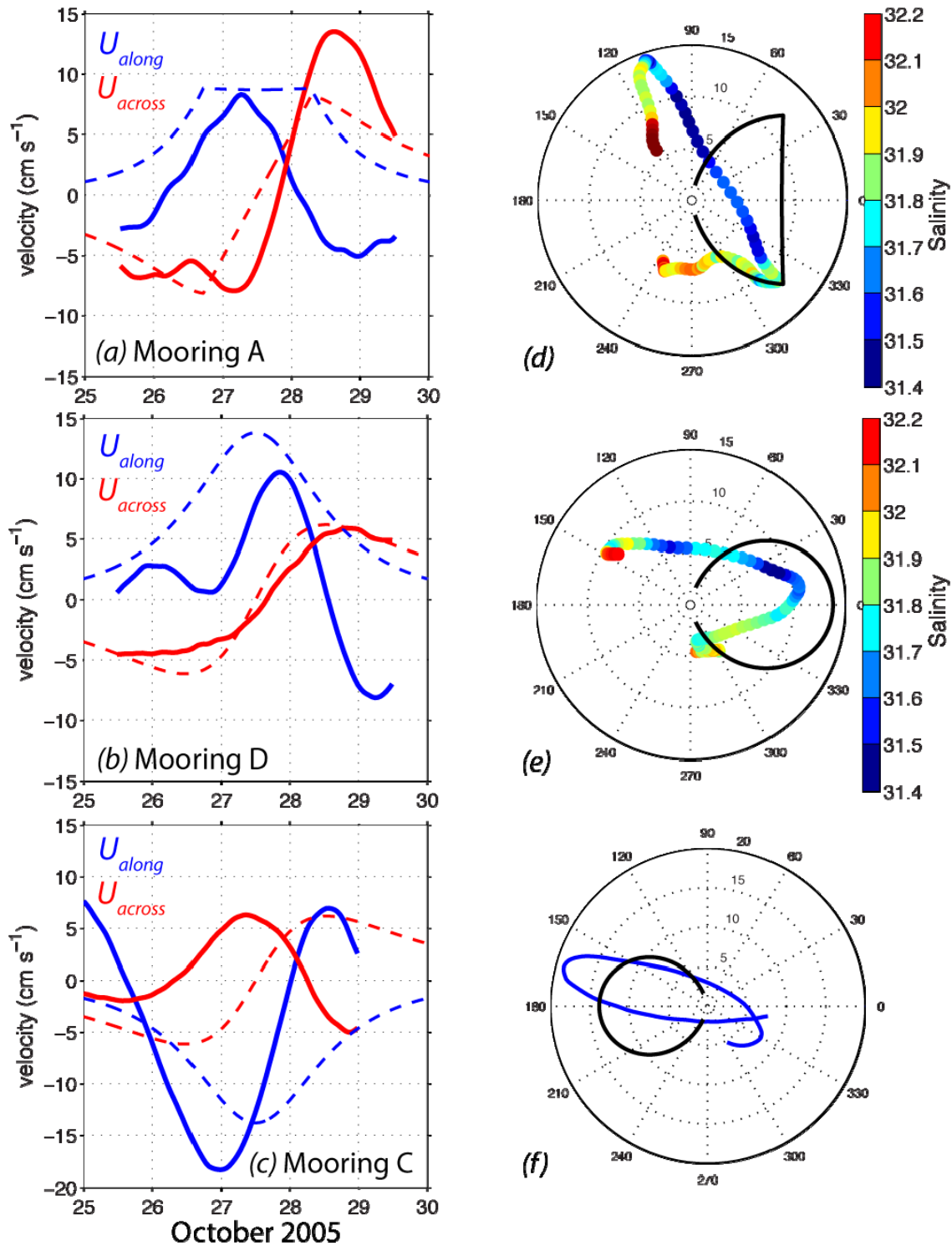
236
 237
 238 **Figure 4.** Time-series of daily maximum ice draft (m) measured by the Upward Looking Sonar
 239 instrument on the center mooring during a three-month period of fall 2005. Shading indicates occurrences
 240 of low-salinity pulses observed by the mooring array.
 241

242 Several mechanisms could explain the propagation of low-salinity water past mooring A
 243 in what appears to be a series of pulses, as well as explain the variations in freshwater transport.
 244 The first mechanism is that variations are caused by the movement of the outflow frontal region

245 back and forth across mooring A (i.e., imagine the 32 isohaline in Fig. 1c oscillating left to right
246 across the mooring). The movement of this front would show up in observations at mooring A as
247 a series of low-salinity pulses as the fresher inshore water moves past the array and back again.
248 A second plausible explanation is that these pulses are due to the freshwater input from different
249 sources both spatially and temporally separated, either caused by wind-induced accelerations of
250 the boundary current in Hudson Bay (Prisenberg, 1987) or by individual river plumes making
251 their way into the Strait. These pulses would show up in the strait as buoyant, anticyclonic eddies
252 propagating by the mooring array. The third mechanism, inherent to the outflow current itself, is
253 that local baroclinic or barotropic instabilities cause the outflow to go unstable and break up into
254 a series of finite low-salinity eddies that then propagate by the moorings.

255 To investigate these possible mechanisms, we next examine the velocity and salinity
256 structure of an event from data taken across the mooring array. The velocity signals shown in
257 Fig. 5, which displays U_{across} and U_{along} for the late October event described above (Fig. 3),
258 displays the records from all three moorings across the outflow, averaged over the upper 60 m.
259 At the two outer moorings (A and D, Fig. 1), the signal in U_{across} is consistent and shows a
260 switching from onshore to offshore flow (Fig. 5a-b). At the inner mooring C, on the other hand,
261 the signal is reversed with offshore flow preceding onshore flow. The zero-crossing of all three
262 U_{across} signals occur at approximately the same time. For U_{along} the observations at mooring A
263 and D are again consistent, with an increase coincident with the switching from onshore to
264 offshore flow, though the exact timing does not agree as well as for U_{across} . Inshore at mooring C,
265 the velocity flowed upstrait during the event (Fig. 5c).

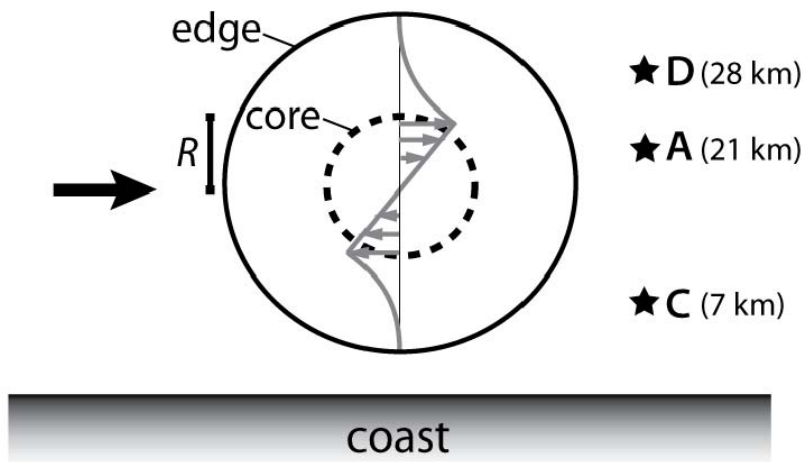
266



267
 268 **Figure 5.** (a) Observed upper layer (0-60 m) velocities (solid lines) at the central mooring for a typical
 269 low-salinity event, compared to theoretical velocities (dashed lines) taken from slicing through a two-
 270 layer eddy north of the eddy center. (b) Same as in a, but for mooring D with the slice north of the eddy
 271 edge. (c) Same as in a, but for mooring C with the slice south of the eddy edge. (d) Hodograph of the
 272 observed velocities in a colored with the salinity at the upper CTD, plotted against the theoretical
 273 velocities in a (black line). (e) Same as in d, but for mooring D. (f) Same as in d, but for mooring C,
 274 where no salinity data was available.

275 Alongside the observed velocities are velocities derived from a simple two-layer eddy
 276 model with a core speed of 0.15 m s^{-1} and a radius of 20 km, corresponding to a passage
 277 timescale of ~ 1.5 days. This model assumes the eddy can be idealized as a Rankine vortex that
 278 has a solid-body core within a radius R and $1/r$ decay elsewhere, where r is the azimuthal
 279 position along the eddy radius (Fig. 6). A similar model was used in the Labrador Sea to
 280 investigate eddies observed by a single mooring (Lilly and Rhines, 2002). As an eddy propagates
 281 by the mooring array, the velocities are taken from the slice that each mooring would measure.
 282 For example, imagine an anticyclonic, surface-trapped eddy propagating through Hudson Strait
 283 such that the center of the eddy passed just south of mooring A ($r < R$), while mooring D
 284 observed the region just north of the eddy edge ($r > R$), and mooring C observed just south of the
 285 eddy edge ($r > R$). Fig. 6 presents a schematic of this situation. The resulting velocities at each
 286 mooring would be those illustrated in Fig. 5, which compare reasonably well to the observed
 287 velocities.

288



289

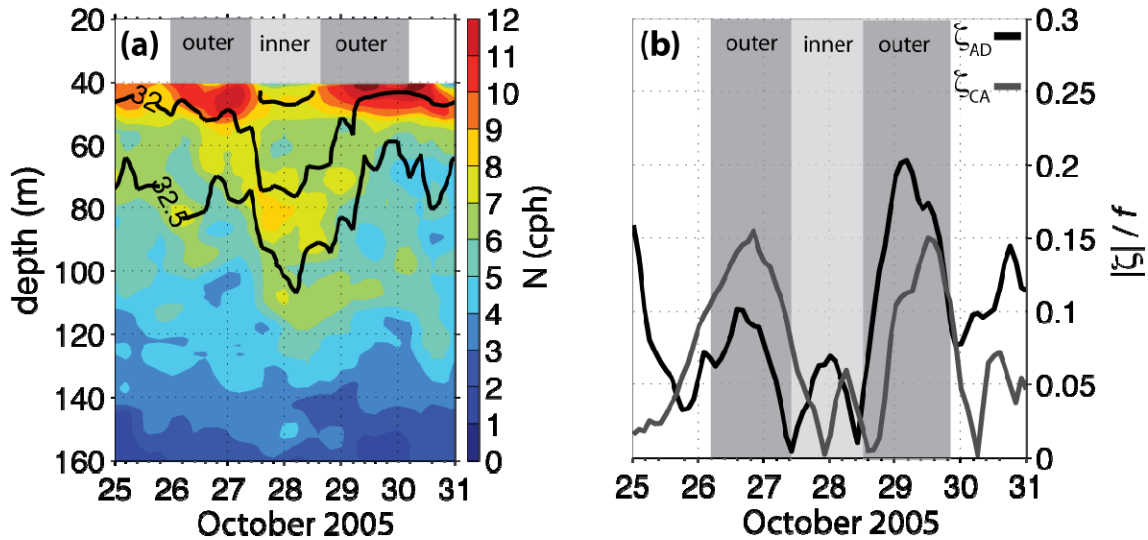
290 **Figure 6.** Schematic of an anticyclonic, low-salinity eddy propagating by the mooring array (shown to approximate
 291 scale, with distances of each mooring given from the coast). The eddy has a core of radius R (dashed circle), a fresh
 292 anomaly out to its edge (solid circle), and is moving from left to right. Gray lines show the velocity structure of an
 293 ideal Rankine vortex.
 294

295 Hodographs of the same data are revealing when plotted with concurrent salinity data
296 from the upper CTDs where available for mooring A and D (Fig. 5d-f). The eddy core appears as
297 a straight line in the theoretical hodograph (Fig. 5d), and the observations show a similar
298 straight-line feature that corresponds to the observed low-salinity water. The observations are
299 consistent at mooring D (Fig. 5e), which shows that the hodograph should be circular for a slice
300 north of the eddy center and that compares well to the observed velocities and low-salinity water.
301 The circle is reversed at mooring C (Fig. 5f), as the inner mooring observes an eddy slice south
302 of the edge and measures oppositely directed flow.

303 All 38 of the identifiable events from Sept. 2005 to Apr. 2006 had a velocity structure
304 qualitatively consistent with the observations shown in Fig. 5. This suggests that these events are
305 anticyclonic eddies with a low-salinity, buoyant core.

306 In addition to the consistent hydrographic and CDOM properties observed during each
307 eddy, the stratification, $N = (-g/\rho_0 \cdot \partial\rho/\partial z)^{1/2}$, of the outflow was higher at depth during times
308 when an eddy was present and propagating by the mooring array. Fig. 7a shows the stratification
309 during the same late October event. Stratification increased in deeper water (~60-120 m range) as
310 the eddy propagated by, and closely matched the salinity contours, but was decreased in the
311 surface core. On the outer edges of the eddy, the gradients were intensified and the highest
312 stratification was observed in the surface waters. The mean stratification over the deep depth
313 range (60-120 m) during the high freshwater transport season (Oct–Jan) was 0.093 cph, while the
314 mean taken over just the times when an eddy was present equaled 0.12 cph (with a standard
315 error, $\sigma = 0.006$, corresponding to 38 events). This stratification anomaly is associated with the
316 hydrographic signal of each low-salinity pulse, which on average over the same depth range (60-
317 120 m), had a salinity anomaly of -0.13 ($\sigma = 0.02$) from the mean S of 32.4, a temperature

318 anomaly of 0.012 ($\sigma = 0.01$) from the mean $T = -0.63^\circ\text{C}$, and a higher CDOM with an anomaly
 319 of 8.8 ppb ($\sigma = 1.7$) over the mean of 280 ppb.
 320



321
 322 **Figure 7.** (a) Observed stratification from the moored profiler (MMP) at mooring A during a typical low-
 323 salinity event that occurred in Oct. 2005, with the inner core of the eddy differentiated from the outer core
 324 (shading). Select isohalines (black lines: 31.5, 32, 32.5) are indicated similarly across all panels. (b) The
 325 absolute value of estimated relative vorticity, ζ , versus time, calculated between moorings A-D (black)
 326 and moorings C-A (gray). ζ is scaled by the Coriolis parameter, f . Shading corresponds to the distinct
 327 eddy regions shown in a.
 328

329 Using the velocity data from the three moorings, we can also estimate the importance of
 330 the relative vorticity, $\zeta = -\partial U_{across}/\partial y + \partial U_{along}/\partial x$, where x, y are the along and across strait
 331 coordinates, respectively. Taking the ratio $|\zeta|/f$ gives a useful measure of the nonlinearity of the
 332 flow. We estimate the $\partial U_{across}/\partial y$ term directly from the ADCP data at the three moorings,
 333 averaged over the upper 80 m in order to use the same depths from all three moorings. The
 334 $\partial U_{along}/\partial x$ term we calculated from the along strait velocities measured at each mooring averaged
 335 over the upper 80 m, and first found $\partial U_{along}/\partial t$. To convert from ∂t to ∂x , we assumed that the
 336 velocity anomalies (i.e., the eddies) were propagated past the mooring array by a slowly-varying
 337 background flow equal to a low-pass filtered U_{along} , calculated using a 7-day Hanning window.

338 The along-strait term was always smaller than the cross-strait term, so the changes to ζ due to the
339 assumptions above were not substantial.

340 Fig. 7b displays the results of these calculations for the time period of late October,
341 during a low-salinity event. Relative vorticity is seen to be significant around the outer core of
342 the eddy, with the maximum ratio $|\zeta|/f = 0.2$. Over the entire fall freshwater season, these ratios
343 ranged from 0–0.45, with the highest values occurring in the intense gradients observed in the
344 outer core of each eddy.

345 Over the eight month period investigated, the mean vertical extent of the 38 events,
346 defined by the 32.2 isohaline, was ~ 75 m ($\sigma = 10$ m), with one event occurring every 4.4 days on
347 average. The mean eddy velocity was ~ 0.19 m s⁻¹ ($\sigma = 0.08$ m s⁻¹ with a large seasonal cycle),
348 calculated as the difference between U_{along} measured at the center of each event at mooring A
349 and the 30-day low-pass filtered U_{along} . Using this velocity scale, we calculated the horizontal
350 extent of each event by converting the time period each event lasted into a distance. The mean
351 horizontal radius was ~ 25 km ($\sigma = 12$ km). This scale is about $3.5L_d$, where $L_d = (g'h)/f$ is the
352 Rossby radius of deformation based on the mean reduced gravity g' and mean vertical extent h .
353 The mean g' was 0.011 m s⁻² ($\sigma = 0.003$ m s⁻²) and was calculated using $g' = g\Delta\rho/\rho_0$, where
354 $\Delta\rho$ is the difference between density measured at the upper and lower CTDs at mooring A, and
355 $\rho_0 = 1025$ kg m⁻³.

356 The effect of the eddies on the freshwater and volume transports of the outflow is
357 significant. If we assume that the outflow velocity is coherent across the mooring array, as
358 observed during 2004-2005 (Straneo and Saucier, 2008a), then we can take the transports
359 calculated at mooring A (Fig. 2a) as a proxy for the entire outflow transports. Removing the time
360 periods when eddies were present results in drastically reduced transport numbers: the volume

361 transport carried by the eddies is 40% of the total, while the freshwater transport contribution is
362 50% of the total.

363

364 **4. Origin of the eddies**

365 The observations displayed in Figs. 3-7 suggest that the synoptic scale variability
366 dominating the MMP salinity record (Fig. 2a) is due to a series of anticyclonic, surface trapped
367 eddies propagating by the mooring array. The frontal movement mechanism would produce a
368 velocity signal in the opposite sense to what is observed at moorings A and D. To test this
369 further, we can calculate the terms in a simple salt balance,

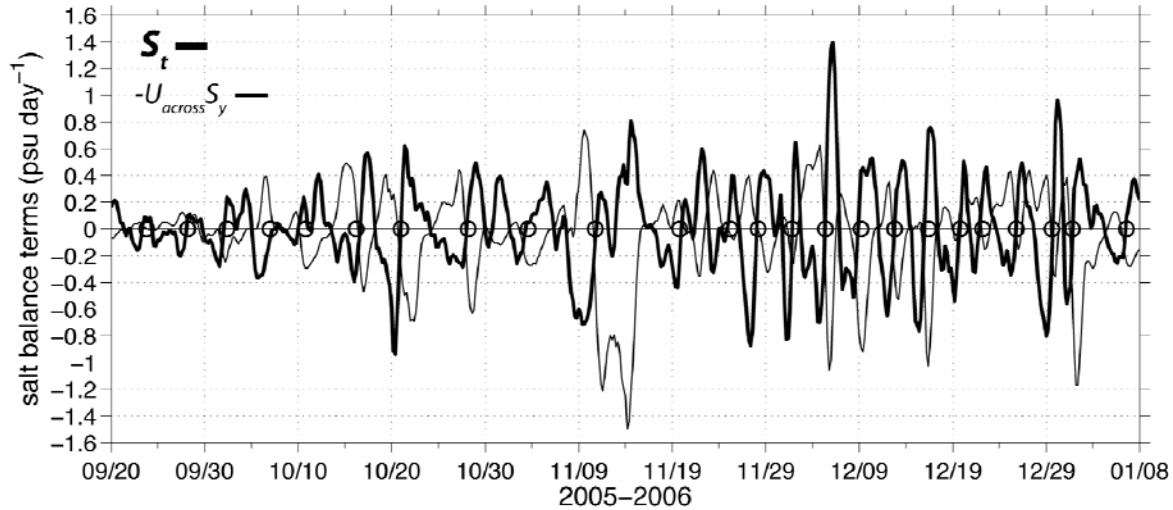
$$370 \quad S_t + U_{across} S_y + U_{along} S_x = 0 \quad (1)$$

371 where subscripts denote partial differentiation in time (t) and in the across (y) and along (x) strait
372 directions. Note that we are neglecting the vertical advection term and any sources or sinks.

373 If the variability was due to movement of the outflow frontal region back and forth across
374 the mooring array, the first two terms in (1) would roughly balance. We can calculate the time
375 rate of change of salinity (S_t) and the across-strait advective term ($U_{across} S_y$) directly from the
376 mooring observations. To do this, we use the observed salinity at 45 m depth at mooring A for S .
377 To calculate the advective term, we use U_{across} at 45 m from mooring A, while the cross-strait
378 salinity gradient is estimated as the difference between the salinity at mooring A at 45 m and that
379 at mooring D. Since there was no instrument at 45 m depth at mooring D, we linearly
380 interpolated between the upper and lower CTDs that were present. The along-strait advective
381 term can only be estimated as a residual between the other two terms.

382 The results of estimating these salt budget terms is shown in Fig. 8 for the first half of the
383 2005-2006 mooring deployment. The timing of each event is marked by an open circle, which

384 corresponds to the zero-crossing of S_t as the observed salinity first decreases, then increases. The
 385 across-strait advective term is, as expected, in the opposite sense to what is needed to balance S_t ,
 386 indicating that frontal movements are not responsible for the observed variability. This implies
 387 that the along-strait advective term must be large enough to balance the residual.
 388



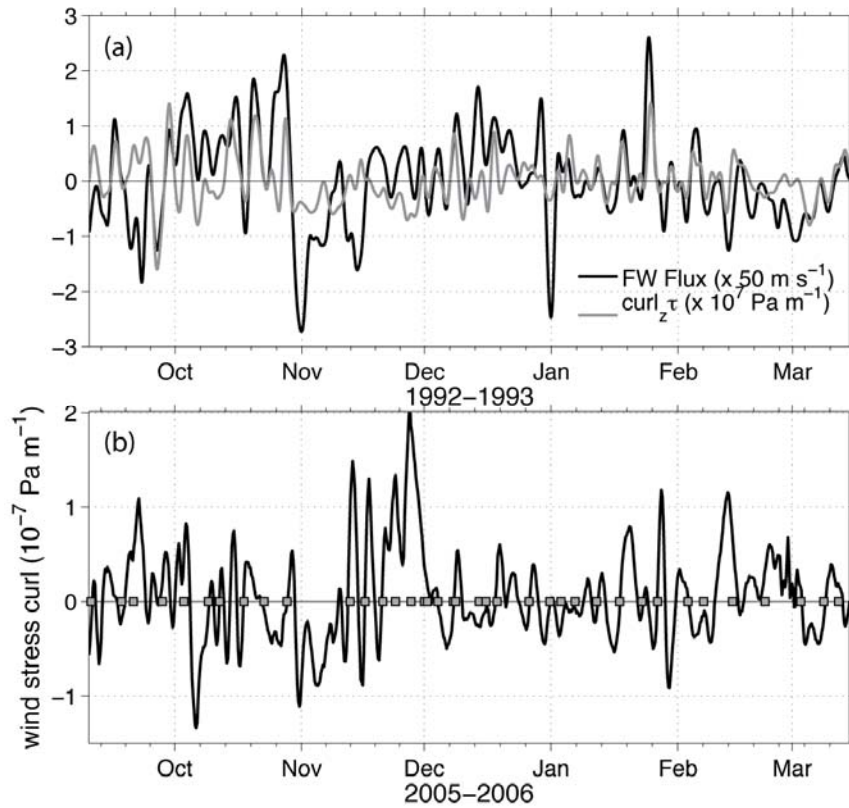
389
 390
 391 **Figure 8.** Two terms (S_t : rate of change of salt, $-U_{across} S_y$: cross-strait advective term) of a simple salt
 392 balance calculated at the central mooring at 45 m depth. The along-strait advective term could not be
 393 estimated from the data. Observed low-salinity events are indicated with open circles.
 394

395
 396 By eliminating the frontal movement mechanism, we are left with either the remotely
 397 forced mechanism, through wind events or individual river discharge events, or the local
 398 instability mechanism, to explain the variability in the Hudson Strait outflow. Previous studies in
 399 Hudson Bay have shown the cyclonic boundary current there to vary synoptically with the
 400 passage of storms over the region, suggesting it is wind-driven (Prisenberg, 1987; Saucier *et al.*,
 401 2004). The modeling study by Saucier *et al.* (2004) further suggested that the head region of
 402 Hudson Strait where Hudson Bay, Foxe Basin, and the strait meet near a tangle of islands and
 403 complex coastal bathymetry (Fig. 1), is a region of intense eddy features and complicated
 404 circulation patterns. In particular, they noted that flow through the constriction between Mansel

405 Island and Quebec (Fig. 1), would stop and go periodically, and was presumably associated with
406 the acceleration of the boundary current to the south of the gap flow. Periodic flow through this
407 gap could generate the anticyclonic, buoyant eddies observed downstream in the Hudson Strait
408 outflow as the cyclonic Hudson Bay boundary current exits into the Strait and turns right under
409 the effects of rotation and buoyancy. The minima in ice draft associated with the majority of the
410 eddies (Fig. 4) supports this hypothesis as well, since waters exiting from southern Hudson Bay
411 during the fall months would tend not to have sea ice cover, as opposed to a more northern origin
412 (e.g., Foxe Basin) for the low-salinity water.

413 To test this hypothesis, we constructed a time series of wind stress curl, $curl_z\tau$, over
414 Hudson Bay to serve as a proxy for the acceleration of the boundary current due to the passage of
415 storms across Hudson Bay. As low-pressure systems move across the bay, positive curl imparts
416 an impulse acceleration to the boundary current on the eastern side of the bay due to northward
417 winds in that region (Prisenberg, 1987; Saucier *et al.*, 2004). At some later time period, the
418 accelerated flow generated by this positive curl moves past Mansel Island and into Hudson Strait
419 to be observed by the mooring array. Support for this process is shown in Fig. 9a, which
420 compares the time series of $curl_z\tau$ with a calculation of freshwater flux from historical mooring
421 data located near Mansel Island in the boundary current (Fig. 1). The data come from a year-long
422 mooring deployment conducted by the Department of Fisheries and Oceans, Canada in 1992-
423 1993. The mooring had a current meter and CTD sensor positioned at 28 m depth, in a total
424 water depth of ~75 m. The freshwater flux time series in Fig. 9a is calculated using the low-pass
425 filtered (34-hr Hanning window) along-channel velocity (approximately northwestward) and the
426 salinity observations collected at the same time. Maximum correlation between the time series

427 was found to be $R = 0.55$ (significant at the 95% level) with $curl_z\tau$ leading the freshwater flux by
 428 1.5 days.



429
 430 **Figure 9.** (a) Time series of wind stress curl, $curl_z\tau$ ($\times 10^7$ Pa m^{-1}), averaged over Hudson Bay and the
 431 freshwater flux ($curl_z\tau$ ($\times 50$ m s^{-1}) calculated from the DFO mooring in 1992-1993. The freshwater flux
 432 estimate is lagged by 1.5 days to show the maximum correlation between the time series. (b) Wind stress
 433 curl, $curl_z\tau$ ($\times 10^{-7}$ Pa m^{-1}), averaged over Hudson Bay calculated from the NCEP reanalysis data for
 434 2005-2006. The timing of low-salinity events observed propagating by the mooring array are shown (gray
 435 squares) lagged by the product of their along-strait speed and the distance to the western entrance of
 436 Hudson Strait (~ 310 km).
 437

438 Fig. 9b displays the low-pass filtered $curl_z\tau$ obtained from the NCEP wind fields
 439 averaged over the entire Hudson Bay region for the 2005-2006 time period. Squares indicate the
 440 lagged time that a low-salinity event was observed to pass by the mooring array. Estimates of the
 441 lag time were calculated using the observed alongstrait velocity at mooring A over the upper 60
 442 m and a length scale of 310 km that is roughly the distance from the head of Hudson Strait to the
 443 mooring array. The velocities used were low-pass filtered with a running 3-day average to

444 remove the effects of the eddy itself and use the speed at which the eddy was propagating at in
445 the outflow current. These lag times ranged from 10-14 days, with the longer times associated
446 with January–April as the outflow slowed down.

447 The results of this calculation show that the lagged pulses are correlated with positive
448 curl, i.e., northward wind acceleration in eastern Hudson Bay. Using the appropriate lag time, 34
449 of the 38 identified low-salinity events observed at the mooring array corresponded to an
450 increase in northward winds in eastern Hudson Bay. This result strongly supports the notion that,
451 indeed, the passage of storms over Hudson Bay and the resulting acceleration of the boundary
452 current there are related to the generation of buoyant eddies that are exported to Hudson Strait.
453 We attribute the discrepancy in the remaining 4 events to either to a difference in origin for the
454 low-salinity waters, i.e. Foxe Basin, which would change the timing of the wind correlation or
455 erase it altogether, or to a difference in mechanism, such as a more local eddy generation induced
456 by baroclinic instability processes that would have no correlation with the wind.

457 Winds in Hudson Bay are correlated to the winds inside the strait, however, so we also
458 tested the correlations between the local wind forcing and the observed velocities in the outflow.
459 Table 1 lists the results of these correlations for U_{along} and U_{across} measured at 45 m at each
460 mooring against V_{wind} . In this case, V_{wind} is taken at a location inside the strait near mooring A at
461 71.3°W, 61.9°N. Significant correlations ($p < 0.05$) were found only at the shallow inner
462 mooring, with maximum correlations in the velocity occurring at a lag of 1 day to the wind
463 forcing. Since no significant correlations were found at mooring A and D, this suggests that local
464 wind forcing is not the cause of the observed velocity fluctuations that characterize the low-
465 salinity events.

466

467 **Table 1.** Correlations of the alongstrait wind obtained from NCEP with the observed upper layer
 468 along- and across-strait velocities (45 m) at the three moorings deployed in 2005-2006. Significant
 469 correlations ($p < 0.05$) are shown in bold. In parentheses is the lag that corresponds to the
 470 maximum correlation when it was significant, otherwise, no significant correlations were found
 471 and the coefficients are for zero lag.

	Mooring C	Mooring A	Mooring D
U_{along}	0.61 (1 day)	0.05	0.01
U_{across}	-0.35 (1 day)	0.15	-0.06

472

473 Of the remaining oceanographic processes that could explain the observed synoptic scale
 474 variability, the individual river plume mechanism is easiest to dismiss. Rivers certainly play a
 475 role in supplying the freshwater for these events and can have strong freshets that are relatively
 476 short-lived. Model results and previous field efforts inside Hudson Bay, though, show the
 477 boundary current to be mixed enough that the distinct rivers feeding the current are lost (Ingram
 478 and Prisenberg, 1998; Saucier *et al.*, 2004; St-Laurent *et al.*, 2010). The properties of the
 479 outflow, with low salinities and high CDOM suggest that the water has a partly riverine origin,
 480 but identifying discrete river freshets would be impossible.

481 On the other hand, the strongly baroclinic velocity and buoyancy signature in the outflow
 482 raises the possibility that local instability processes could be a cause for the observed variability.
 483 The baroclinic and barotropic instability mechanisms are difficult to diagnose with limited
 484 observations, although many coastal currents previously studied, such as the Norwegian Coastal
 485 Current (Mork, 1981), the East Greenland Coastal Current (Sutherland and Pickart, 2008), the
 486 flow off Cape Cod, USA (Shcherbina and Gawarkiewicz, 2008) and the western Arctic
 487 shelfbreak current (Spall *et al.*, 2008) have been observed to show variations associated with
 488 baroclinic instabilities. Theoretical scales can be estimated from the limited hydrographic section

489 data to constrain the growth rates and corresponding horizontal scales of the baroclinic instability
490 process.

491 For example, the slope Burger number, $Sl = \alpha N / f$, where α is the bathymetric slope is a
492 measure of the buoyant current structure, with $Sl \ll 1$ indicating a slope-controlled regime and
493 $Sl \gg 1$ indicating a surface-trapped current (Lentz and Helfrich, 2002). Taking typical values for
494 the Hudson Strait outflow, $\alpha = 0.01$, $f = 1.3 \cdot 10^{-4} \text{ s}^{-1}$, and a stratification range of $N = 0.0066\text{--}$
495 0.010 s^{-1} , gives $Sl \sim 0.5\text{--}0.7$, suggesting the outflow is in the slope-controlled regime of buoyant
496 currents. Slope-controlled currents tend to be more stable than buoyant currents against a vertical
497 wall (Lentz and Helfrich, 2002). A related parameter to investigate this stability is $\delta = \alpha / \partial\rho/\partial z$,
498 the ratio of the bottom slope to the isopycnal slope. Typically, $\delta < 0$ for buoyant currents
499 (Shcherbina and Gawarkiewicz, 2008; Blumsack and Gierasch, 1972). For Hudson Strait, given
500 the typical bottom slope, $\alpha = 0.01$, and an isopycnal slope estimated from hydrography using the
501 32 isohaline (Fig. 1c), $\delta \approx -2$. Given that value of δ , we can estimate the maximum growth rate
502 and length scale of baroclinic instability (following equations 3.12 and 3.13 of Blumsack and
503 Gierasch, 1972; also see Shcherbina and Gawarkiewicz, 2008), which are 5.8 days^{-1} and 2.0 km ,
504 respectively. The length scale corresponds to a wavelength of $2\pi \cdot 2.0 \text{ km} \sim 12.9 \text{ km}$, which is \sim
505 $1.6L_d$. Thus, the range of scales due to a baroclinic instability mechanism are plausible given the
506 observed scales of the eddies, but a detailed stability analysis and discussion of the instabilities is
507 beyond the scope of this paper.

508

509 **5. Conclusions and summary**

510 The series of discrete, low-salinity pulses observed in the Hudson Strait outflow are
511 surface-trapped, anticyclonic eddies with vertically and horizontally coherent salinity, CDOM,

512 and velocity signals. These eddies carry approximately half of the freshwater transport and 40%
513 of the volume transport through Hudson Strait. This is an important result as it represents a
514 different form of freshwater transport, compared to the conventional view of a continuous coastal
515 current outflow from Hudson Bay. Since the freshwater outflow modulates how high-
516 stratification and high-nutrient water enters the northern North Atlantic, and the highly
517 productive Labrador shelf region in particular, the fact that the outflow is confined to coherent
518 eddy-like structures that preserve their properties for longer periods of time is a critical point.

519 We find that the timing of these eddies can be explained by atmospheric variability over
520 Hudson Bay, due to the passage of storms over the bay that force low-salinity boundary current
521 waters out near Mansel Island. Whether or not the inflow on the northern side of the strait
522 exhibits similar synoptic variability, or is influenced by the propagation of these eddies in the
523 outflow, is an open question. Another uncertainty is what the spatial and temporal alongstrait
524 variations in salinity are in Hudson Strait. Observational efforts are underway to explore the first
525 of these questions, with moorings placed in the barotropic inflow last year. However, models
526 may provide the most useful insight into quantifying the alongstrait variability, though they must
527 be of high enough resolution to resolve the mesoscale features we observe.

528

529 **Acknowledgments**

530 This work was funded by National Science Foundation grant OCE-0751554. Special gratitude to
531 Jim Ryder, the Canadian Coast Guard ships and crew who helped deploy and recover the
532 moorings in Hudson Strait. The authors also thank Emmanuel Boss for insights on the CDOM
533 data, and Andrey Shcherbina and Rocky Geyer for useful comments.

References

- Arbic, B.K., P. St-Laurent, G. Sutherland, and C. Garrett, 2007. On the resonance and influence of the tides in Ungava Bay and Hudson Strait. *Geophys. Res. Lett.*, *34*, doi:10.1029/2007GL030845.
- Blumsack, S.L., and P.J. Gierasch, 1972. Mars: The effects of topography on baroclinic instability. *J. Atmos. Sci.*, *29*, 1081–1089.
- Déry, S.J., M. Stieglitz, E.C. McKenna, and E.F. Wood, 2005. Characteristics and trends of river discharge into Hudson, James, and Ungava bays, 1964–2000. *J. Climate*, *18*, 2550–2557.
- Dickson, R., J. Meincke, P.B. Rhines, 2008. Arctic-Subarctic Ocean Fluxes: Defining the Role of the Northern Seas in Climate. Springer, 738 pp.
- Dickson, R., B. Rudels, S. Dye, M. Karcher, J. Meincke, and I. Yashayaev, 2007. Current estimates of freshwater flux through Arctic and subarctic seas. *Prog. Oceanogr.*, *73*, 210–230.
- Drinkwater, K.F., 1988. On the mean and tidal currents in Hudson Strait. *Atmos.-Ocean.*, *26*, 252–266.
- Drinkwater, K.F., and G.C. Harding, 2001. Effects of the Hudson Strait outflow on the biology of the Labrador Shelf. *Can. J. Fish. Aquat. Sci.*, *58*, 171–184.
- Egbert, G.D., and R.D. Ray, 2001. Estimates of M_2 tidal energy dissipation from TOPEX/Poseidon altimeter data. *J. Geophys. Res.*, *106*, 22,475–22,502.
- Gagnon, A.S., and W.A. Gough, 2005. Trends in the dates of freeze-up and breakup over Hudson Bay, Canada. *Arctic*, *58*, 370–382.
- Ingram, R.G. and S.J. Prisenberg, 1998. Coastal oceanography of Hudson Bay and surrounding Eastern Canadian Arctic waters, *in* The Sea, Vol. 11, The Global Coastal Ocean, Regional Studies and Synthesis. Robinson and Brink, ed., 835–861.
- Large, W.G. and S. Pond, 1981. Open ocean momentum flux measurements in moderate to strong winds. *J. Phys. Oceanogr.*, *11*, 324–336.
- Lentz, S.J. and J. Largier, 2006. The influence of wind forcing on the Chesapeake Bay buoyant coastal current. *J. Phys. Oceanogr.*, *36*, 1305–1316.
- Lilly, J.M., and P.B. Rhines, 2002. Coherent eddies in the Labrador Sea observed from a mooring. *J. Phys. Oceanogr.*, *32*, 585–598.
- Mork, M., 1981. Circulation phenomena and frontal dynamics of the Norwegian Coastal Current. *Phil. Trans. Royal Soc. Lond., Ser. A*, *302*, 635–647.
- Pawlowicz, R., R. Beardsley, and S. Lentz, 2002. Classical tidal harmonic analysis including error estimates in MATLAB using T_TIDE. *Comp. and Geosci.*, *28*, 929–937.
- Prisenberg, S.J., 1987. Seasonal current variations observed in western Hudson Bay. *J. Geophys. Res.*, *92*, 10,756–10,766.
- Saucier, F.J., S. Senneville, S. Prisenberg, F. Roy, G. Smith, P. Gachon, D. Caya, and R. Laprise, 2004. Modelling the sea ice-ocean seasonal cycle in Hudson Bay, Foxe Basin and Hudson Strait, Canada. *Clim. Dynamics*, *23*, 303–326.
- Serreze, M.C., A.P. Barrett, A.G. Slater, R.A. Woodgate, K. Aagaard, R.B. Lammers, M. Steele, R. Moritz, M. Meredith, and C.M. Lee, 2006. The large-scale freshwater cycle of the Arctic. *J. Geophys. Res.*, *111*, doi:10.1029/2005JC003424.
- Shcherbina, A.Y., and G.G. Gawarkiewicz, 2008. A coastal current in winter: Autonomous underwater vehicle observations of the coastal current east of Cape Cod. *J. Geophys. Res.*, *113*, C07030, doi:10.1029/2007JC004306.

- Spall, M., R. S. Pickart, P. Fratantoni, and A. Plueddemann, 2008. Western Arctic shelfbreak eddies: formation and transport. *J. Phys. Oceanogr.*, 38, 1644-1668.
- St-Laurent, P., F. Straneo, J.-F. Dumais, and D.G. Barber, 2010. What is the fate of the river waters of Hudson Bay. *J. Mar. Res.*, xxx, xxx, this issue.
- Straneo, F. and F. Saucier, 2008*a*. The outflow from Hudson Strait and its contribution to Labrador Current. *Deep-Sea Res. I*, doi:10.1016/j.dsr.2008.03.012.
- Straneo, F. and F. Saucier, 2008*b*. The arctic-sub arctic exchange through Hudson Strait, *in* Arctic-Subarctic ocean fluxes: Defining the role of the Northern Seas in climate. Dickson, Meincke, and Rhines, ed., 740 pp.
- Straneo, F., et al. 2010. Interannual variations in the freshwater and heat transport from Hudson Bay, 2004-2007. *J. Mar. Res.*, xxx, xxx, this issue.
- Sutcliffe, W.H., Jr., R.H. Loucks, K.F. Drinkwater, and A.R. Coote, 1983. Nutrient flux onto the Labrador Shelf from Hudson Strait and its biological consequences. *Can. J. Fish. Aquat. Sci.*, 40, 1692–1701.
- Sutherland, D.A., and R.S. Pickart, 2008. The East Greenland Coastal Current: structure, variability, and forcing. *Prog. Oceanogr.*, doi:10.1016/j.pocean.2007.09.006.